Supplementary Materials

Ruiming Guo and Thierry Blu
Department of Electronic Engineering, The Chinese University of Hong Kong
1155100873@link.cuhk.edu.hk, thierry.blu@m4x.org

I. Rotational continuity

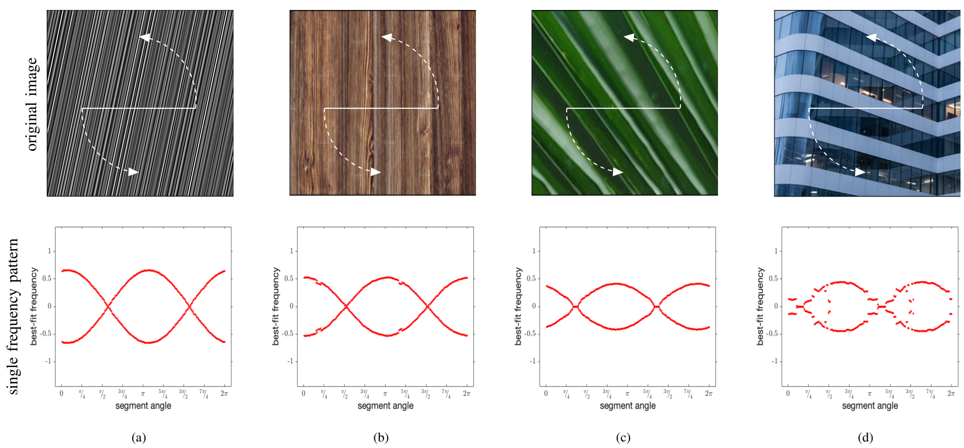

Fig. 1: **Successful examples.** From top to bottom: test images; estimated 1D scaling features; denoised 1D scaling features. From left to right: (a) Stationary laminar image. The 1D signal along $\boldsymbol{u}$ is white noise which is stationary; (b) Wood grain; (c) Needle Leaves; (d) Building. We can observe there are deterministic patterns in the raw 1D scaling features (second row).

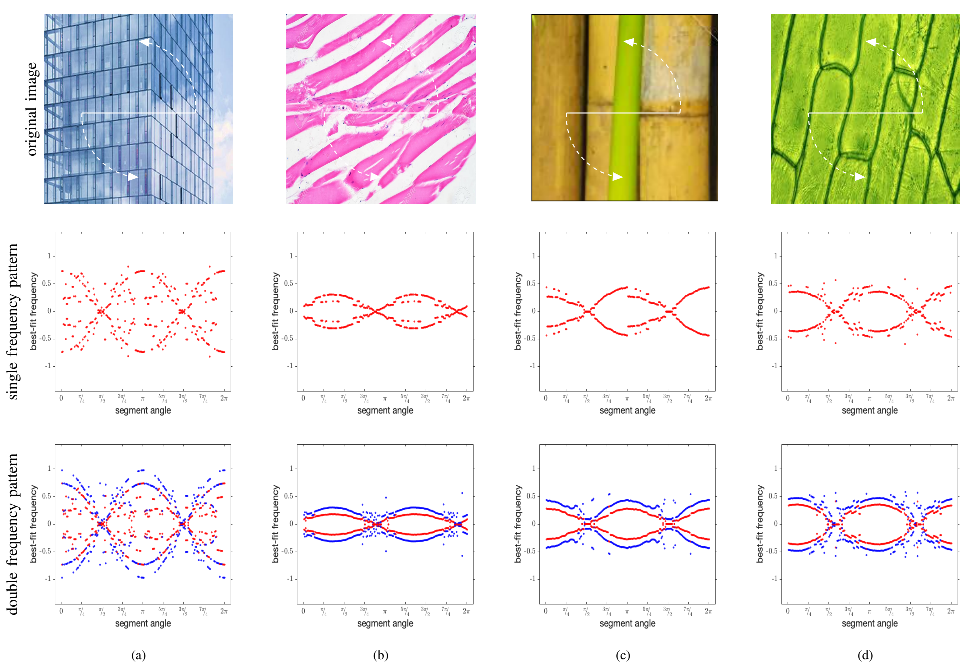

Fig. 2: **Less successful examples.** From top to bottom: test images; estimated 1D scaling features; desnoised 1D scaling features. (a) High-rise building facades; (b) Muscle tissue; (c) Bamboo grove; (d) Plant cells. Obviously, the rotation patterns in these figures are either more unclear or local.

II. Robustness of the sinusoid fitting error to noise

Fig. 3 shows how the sinusoid-fitting error $\left||\hat{\omega}| - |\omega_g \mathbf{u}^\mathsf{T}\mathbf{a}|\right|$ changes with the scalar product $|\mathbf{u}^\mathsf{T}\mathbf{a}|$ (with $\|\mathbf{a}\|_2 = 1$) when we add noise to the laminar image (0 dB here). To better visualize the spread of this error, as well as its overall amplitude, 10 realizations (by randomly shifting the laminar image) are processed for each value of $|\mathbf{u}^\mathsf{T}\mathbf{a}|$. The corresponding image conditioning $\hat{\lambda}$ is: 1.640. The other quantities involved in Corollary 1 are left unchanged: $\omega_g = 0.2$, $T = 41$, $\Delta_0 = 0.7$, $\Delta_1 = 1.2$ and $\gamma_0 = 0.67$.

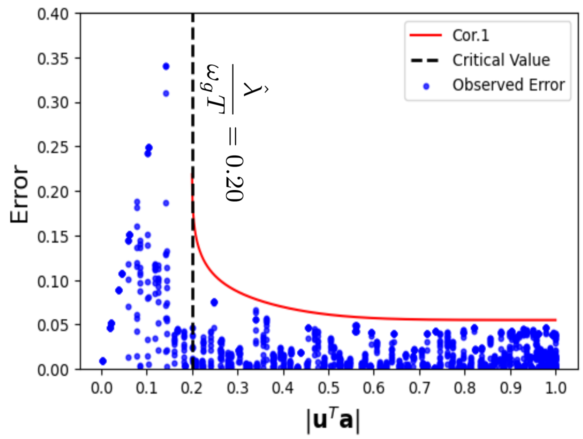

Fig. 3: Effect of the noise: noise (PSNR $= 0$ dB) is added to the laminar image. Despite that, the plot of the frequency estimation error in function of the slope of the line shows little change with the noiseless case, for which Corollary 1 provides an upper bound when $|\mathbf{u}^\mathsf{T}\mathbf{a}| > \hat{\lambda}/(\omega_g T)$ (approximate $\hat{\lambda}/(\omega_g T)$ value is also 0.20).

III. Accuracy of the curve reconstruction in the presence of noise

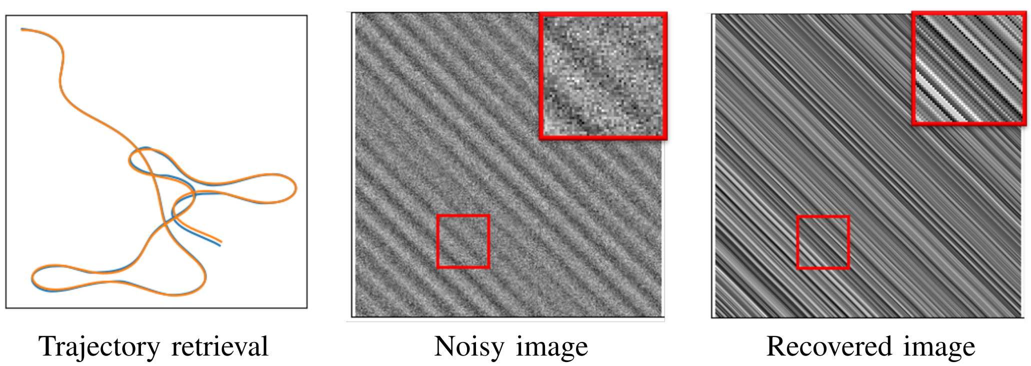

Fig. 4: Retrieval of a trajectory in the presence of noise. Left: ground-truth (red) and estimated (blue) trajectory; center: the noisy laminar image (0 dB noise); right: reconstructed laminar image ($\mathrm{err}_{\mathrm{trajectory}} = 4.82$ pixels, $\mathrm{err}_{\mathrm{samples}} = 5.54$ dB compared to the noiseless samples).

As mentioned in visual intuition section, the best-fit frequency is very robust to noise, which enables the trajectory retrieval from very noisy 1D samples. Here, we show what happens when the image is corrupted by strong white noise (PSNR $= 0$ dB). Thanks to the quadratic-fitting strategy, the separated outliers can be robustly removed, which gives rise to a clean frequency estimation (see Fig. 4). Hence, despite the strong noise, the trajectory can be accurately retrieved with a small reconstruction error $\mathrm{err}_{\mathrm{trajectory}} = 4.82$ pixels. In that case, $\mathrm{err}_{\mathrm{samples}} = 5.54$ dB is quite poor, likely because the noisy image is not laminar anymore, whereas its reconstruction is PSNR $= 13.08$ dB. The laminar image is kept unchanged from the previous experiments: $\omega_g = 0.2$, $T = 41$, $\Delta_0 = 0.7$, $\Delta_1 = 1.2$, and $\gamma_0 = 0.5$, which leads to $\hat{\lambda} = 0.902$. And the trajectory is set as $\kappa_{\max} = 0.010$.

IV. Sinusoid Fitting Algorithm

Theorem 1. *Consider the 1D samples $s_n, n = 1, 2, \cdots, N, s_n \in \mathbb{R}$. The mimimum of the mean-square fit criterion*

$$J(A, \omega) = \sum_{n=1}^{N} |s_n - Ae^{j\omega n}|^2 \tag{1}$$

over $A \in \mathbb{C}$ and $\omega \in]-\pi, \pi]$ is attained for a value of ω that satisfies $P(e^{j\omega}) = 0$, where P is the polynomial defined by

$$P(X) = \sum_{n=-N+1}^{N-1} n c_n X^{N+n+1}$$

and where $c_n = \sum_k s_k s_{k+n} = c_{-n}$ is the autocorrelation sequence of the samples s_n.

Proof. Minimizing the criterion over A results in

$$A(\omega) = \frac{1}{N} \sum_{n=1}^{N} s_n e^{-j\omega n}.$$

Then, substituting $A(\omega)$ into the criterion (1) results in

$$J(A(\omega), \omega) = \sum_{n=1}^{H} |s_n|^2 - \frac{1}{N} \Big| \sum_{n=1}^{N} s_n e^{-j\omega n} \Big|^2.$$

Minimizing this expression w.r.t. ω amounts to maximizing

$$\begin{aligned} J_0(\omega) &= \frac{1}{N} \Big| \sum_{n=1}^{N} s_n e^{-j\omega n} \Big|^2 \\ &= \sum_{n=-N+1}^{N-1} c_n e^{j\omega n}. \end{aligned}$$

This minimum is attained when the derivative $\sum_{n=-N+1}^{N-1} jnc_n e^{j\omega n}$ vanishes, which is equivalent to $P(e^{j\omega}) = 0$. $\square$

Hence, an exact algorithm for minimizing $J(A, \omega)$ consists in

1) calculating c_n, the autocorrelation of s_n
2) finding all the roots of $P(X)$ that are of modulus 1 ($X = 1$ is always one of them)
3) rank these roots based on $\left| \sum_{n=1}^{N} s_n X^n \right|$

The result eventually consists in two complex conjugate solutions: X_0 and X_0^*, the phase of which are the value of ω and $-\omega$ which are the solutions of the minimization problem.

A key point of this polynomial roots finding algorithm is that the number of maxima is finite and known (equal to $2N - 2$), which guarantees that the result obtained is optimal. This makes it as an exact algorithm.

In practice, an efficient implementation of this algorithm can be achieved by using the FFT (Fast Fourier Transform) algorithm: extending the N samples s_n to, e.g., 4096 by padding with zeros and selecting the absolute maximum of the FFT of these extended samples provides an approximate solution which is a sufficiently accurate for our purpose, while being very efficient computationally. And, obviously, this approximate calculation does not suffer from the potential inaccuracy caused by the polynomial root-finding algorithm needed in (1)—typically, when the sample size N becomes larger than $\simeq 200$.

V. Reconstruction Hypotheses

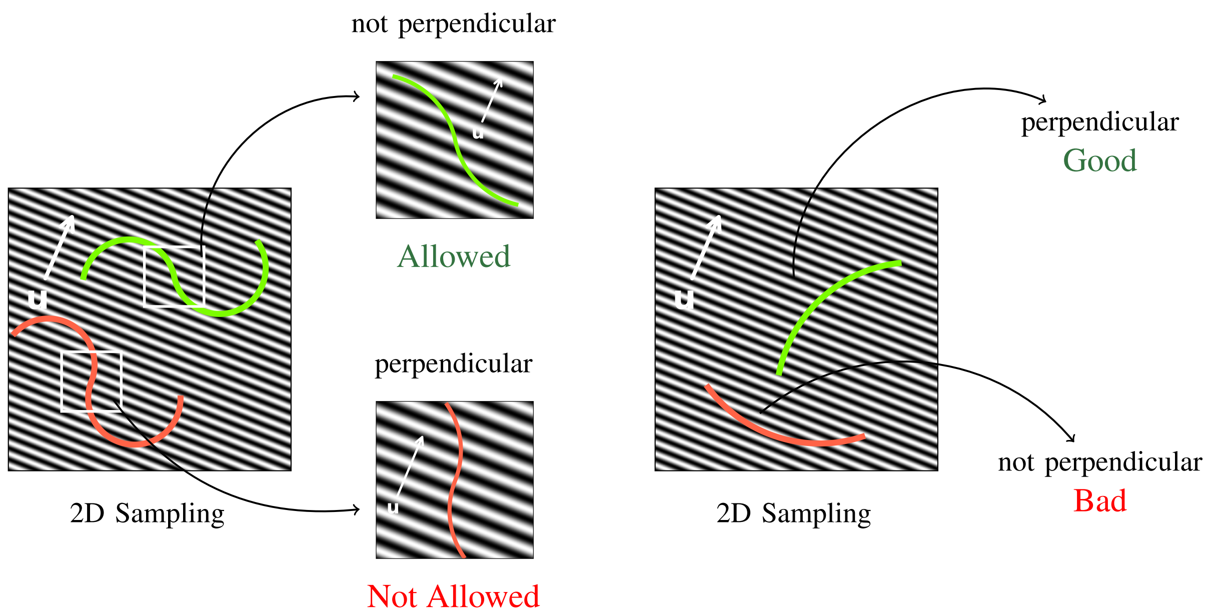

(a) Inflection points (b) Crossing of the laminar direction

Fig. 5: Geometric assumptions on the mobile trajectory.

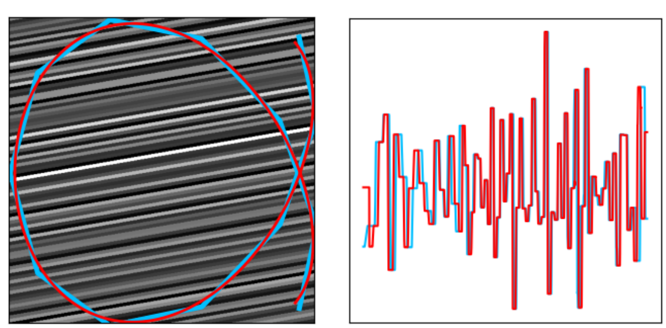

(a) (b)

Fig. 6: Linear approximation of non-straight line sampling: (a) Piecewise linear approximation (blue) of the curved trajectory (red). (b) The resulting approximate 1D time series (red: ground truth, blue: approximate).